






Braiding Majoranas in a linear quantum dot-superconductor array: Mitigating the errors from Coulomb repulsion and residual tunneling

Sebastian Miles ^{1,*} Francesco Zatelli ¹ A. Mert Bozkurt ¹ Michael Wimmer ¹ and Chun-Xiao Liu ^{1,†}

¹*QuTech and Kavli Institute of Nanoscience, Delft University of Technology, Delft 2600 GA, The Netherlands*

(Dated: January 28, 2025)

Exchanging the positions of two non-Abelian anyons transforms between many-body wavefunctions within a degenerate ground-state manifold. This behavior is fundamentally distinct from fermions, bosons and Abelian anyons. Recently, quantum dot-superconductor arrays have emerged as a promising platform for creating topological Kitaev chains that can host non-Abelian Majorana zero modes. In this work, we propose a minimal braiding setup in a linear array of quantum dots consisting of two minimal Kitaev chains coupled through an ancillary, normal quantum dot. We focus on the physical effects that are peculiar to quantum dot devices, such as interdot Coulomb repulsion and residual single electron tunneling. We find that the errors caused by either of these effects can be efficiently mitigated by optimal control of the ancillary quantum dot that mediates the exchange of the non-Abelian anyons. Moreover, we propose experimentally accessible methods to find this optimal operating regime and predict signatures of a successful Majorana braiding experiment.

I. INTRODUCTION

The exchange statistics of identical particles is a central concept in quantum mechanics. It allows for classifying elementary particles (e.g., electrons and photons) into fermions and bosons. In lower-dimensional spaces, there exist more exotic particles, e.g., non-Abelian anyons [1, 2]. By exchanging the positions of two such anyons, referred to as a braid operation, the many-body wavefunction transforms into a different one in the degenerate ground-state manifold. Thus, applying the same set of braid operations in a different order results in different unitary evolutions of the system. In addition, non-Abelian anyons are regarded as the building blocks of topological quantum computation, where qubit information is encoded in a pair of anyons, and quantum gates are implemented by anyonic braiding [2, 3]. Ideally, this protocol is intrinsically fault-tolerant, because both storage and processing of the quantum information are immune to local perturbations due to the topological protection. Therefore, demonstrating non-Abelian exchange statistics is of great importance to fundamental physics as well as to topological quantum computation.

Majorana zero modes, which are Ising anyons, are the simplest example of non-Abelian anyons [3–14]. They can appear at the defects of a topological superconductor in the form of a mid-gap quasiparticle excitation [15–18]. In particular, it was proposed that topological Kitaev chains and Majorana zero modes can be engineered in a quantum-dot-superconductor array using a bottom-up approach [19]. An advantage of this proposal is the intrinsic robustness against the effect of disorder that is ubiquitous in mesoscopic systems [20–22]. Moreover, by controlling the relative strengths of normal and su-

perconducting couplings between neighboring quantum dots [23, 24], it is even possible to create Majoranas in the short-chain limit [25], albeit lacking true topological protection in this case. Based on these proposals, significant experimental progress has been achieved recently in realizing short Kitaev chains in two- [26–28] and three-quantum-dot chains [29–31], supported by tunnel spectroscopy evidence of Majorana zero modes at finely tuned sweet spots. This opened up a new research field for Majorana physics and topological superconductivity [23, 32–55]. It also provides a new and promising platform to demonstrate the non-Abelian character of the exchange statistics [56–59], which has been elusive for decades.

In quasi-one-dimensional systems, braid operations can also be implemented by cyclic tuning of the pairwise Majorana couplings in a trijunction [60–63], or by a sequence of measurement on the fermion parity in Majorana pairs [64–66], both of which are mathematically equivalent to physically moving Majoranas in a T -junction [67]. Furthermore, it was shown that the setup of trijunction braiding can be further simplified, where the role of a vertical topological superconductor branch can be replaced by a quantum dot [68–70]. However, it is a critical open question whether a braid protocol proposed for Majorana nanowires remains valid in the quantum dot setups with strong interactions. For example, it has been recently shown that strong interdot Coulomb interaction can prevent the extraction of Majorana quality measures [34], and that Coulomb interaction within a Kitaev chain can be detrimental to the protection of Majorana zero modes or qubits [25, 47, 50].

In the current work, we generalize the minimal braid protocol to engineered Kitaev chains, focusing on the physical effects that are peculiar to quantum dot devices, e.g., strong interdot Coulomb repulsion and residual single-electron tunneling. Surprisingly, we find that the detrimental errors caused by both effects can be efficiently mitigated by optimal control of the ancillary quantum dot. Moreover, we propose experimentally ac-

* s.miles@tudelft.nl

† chunxiaoliu62@gmail.com

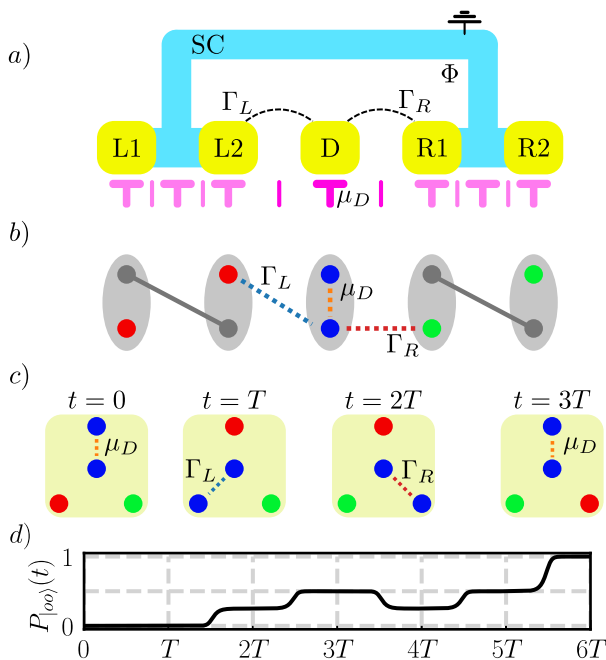


FIG. 1. (a) Schematic of the minimal setup required for braiding in a linear array of quantum dots. Yellow squares are normal quantum dots, blue regions are superconducting leads mediating normal and Andreev tunneling. Purple lines are electrostatic gates to control the parameters. (b) Majorana representation of the Hamiltonian: The grey ovals with filled circles represent the Majorana operators $\gamma_{a,A/B}$ for dot a , lines represent effective couplings. By tuning its chemical potential, the ancillary dot D supplies two Majoranas forming a virtual trijunction together with dots $L2$ and $R1$. (c) Schematic of the single Majorana exchange protocol. A full braid is implemented by varying μ_D , Γ_L , and Γ_R in sequence twice. μ_D , Γ_L , and Γ_R can be experimentally controlled via three electrostatic gates (dark purple). (d) Occupation probability of the $|00\rangle$ state depending on t over a full braiding operation. At times $3T$ and $6T$ the protocol implements exchange and full braid of the two Majoranas neighboring the ancillary dot respectively. The line highlights the change in parity the system undergoes during the protocol.

cessible methods to find this optimal operating regime and predict signatures of a successful Majorana braiding experiment.

II. SETUP AND MODEL HAMILTONIAN

The minimal braiding setup in a linear array of quantum dots consists of two copies of a two-site Kitaev chain connected by an ancillary quantum dot in the middle. A schematic of this setup is shown in Fig. 1(a). The model

Hamiltonian is

$$\begin{aligned}
 H &= H_L + H_R + H_D + H_{\text{tunnel}} + H_{\text{Coulomb}}, \\
 H_a &= \sum_{i=1,2} \mu_{ai} n_{ai} + t_a c_{a2}^\dagger c_{a1} + \Delta_a c_{a2} c_{a1} + h.c., \\
 H_D &= \mu_D n_D, \\
 H_{\text{tunnel}} &= \Gamma_L c_D^\dagger c_{L2} + \Gamma_R e^{i\varphi/2} c_D^\dagger c_{R1} + h.c., \\
 H_{\text{Coulomb}} &= U_L n_D n_{L2} + U_R n_D n_{R1}.
 \end{aligned} \tag{1}$$

Here H_a with $a = L/R$ are the Kitaev chain Hamiltonians, c_{ai} and $n_{ai} = c_{ai}^\dagger c_{ai}$ are the annihilation and number operators of the dot orbitals, μ_{ai} is the orbital energy, and t_a and Δ_a are the normal and Andreev tunnelings. H_D is the Hamiltonian for the ancillary quantum dot. Here we assume that both the magnetic-field-induced Zeeman energy and the level spacing are large, such that all quantum dots are in the spinless regime. The effect of on-site Coulomb interaction can thus be safely neglected. H_{tunnel} describes single electron transfer between the end of the Kitaev chain and the ancillary quantum dot, with $\Gamma_{L/R}$ being the tunneling amplitudes. φ is the phase difference between the two superconducting leads, which can be controlled by the magnetic flux Φ through the loop. Here we choose a gauge such that $t_a, \Delta_a > 0$. H_{Coulomb} describes the interdot Coulomb interaction between the inner dots of the Kitaev chains and the ancillary dot. We neglect Coulomb interaction between two dots of the same chain due to the strong screening effect of the grounded superconductor.

III. MINIMAL MAJORANA BRAIDING IN A QUANTUM DOT CHAIN

A. Effective trijunction in the Majorana representation

One of the key results of Refs. 68 and 69 was that a quantum dot forming a junction between two Majorana bound states behaves as an effective tri-junction at a phase difference of π . Here, we briefly show how this argument applies to the quantum dot chain.

To this end, we rewrite the Hamiltonian (1) in the Majorana basis. For each dot, we transform the fermionic operators into Majorana operators as

$$c_a = (\gamma_{aA} + i\gamma_{aB})/2, \quad c_a^\dagger = (\gamma_{aA} - i\gamma_{aB})/2. \tag{2}$$

At the sweet spot of the Kitaev chain we have

$$H_L + H_R = i\Delta_L \gamma_{L2A} \gamma_{L1B} + i\Delta_R \gamma_{R2A} \gamma_{R1B}, \tag{3}$$

with unpaired Majoranas $\gamma_{L1A}, \gamma_{L2B}, \gamma_{R1A}, \gamma_{R2B}$. On the other hand, the Hamiltonian for the ancillary dot reads

$$H_D = i \frac{\mu_D}{2} \gamma_{DA} \gamma_{DB}. \tag{4}$$

The left tunneling Hamiltonian can be rewritten as

$$H_{tunn,L} = i\frac{\Gamma_L}{2}(\gamma_{L2A}\gamma_{DB} - \gamma_{L2B}\gamma_{DA}) \approx -i\frac{\Gamma_L}{2}\gamma_{L2B}\gamma_{DA} \quad (5)$$

where the approximation is to project away the coupling to the high-energy Majorana when $\Delta_L \gg \Gamma_L$. For the right tunneling Hamiltonian, at $\varphi = \pi$, we have equally

$$H_{tunn,R} = i\frac{\Gamma_R}{2}(\gamma_{R1A}\gamma_{DA} + \gamma_{R1B}\gamma_{DB}) \approx i\frac{\Gamma_R}{2}\gamma_{R1A}\gamma_{DA}. \quad (6)$$

Thus the effective Hamiltonian is

$$H_{\text{eff}} = i\frac{\mu_D}{2}\gamma_{DA}\gamma_{DB} - i\frac{\Gamma_L}{2}\gamma_{L2B}\gamma_{DA} - i\frac{\Gamma_R}{2}\gamma_{R1A}\gamma_{DA}, \quad (7)$$

and thus equivalent to a Majorana trijunction [61], and schematically shown in Fig. 1(b). Here, the dot energy μ_D plays effectively the role of a Majorana coupling.

B. Braiding in the ideal case

We first consider an ideal scenario for Majorana braiding. Assuming no interdot Coulomb interaction ($U_L = U_R = 0$), two finely tuned Kitaev chains ($\mu_{ai} = 0$ and $t_a = \Delta_a$) can host four zero-energy Majoranas

$$\gamma_1 = \gamma_{L1A}, \gamma_2 = \gamma_{L2B}, \gamma_3 = \gamma_{R1A}, \gamma_4 = \gamma_{R2B}, \quad (8)$$

localized on four different quantum dots. They form the degenerate ground-state manifold. As shown above, when the phase condition $\varphi = \pi$ is satisfied, Majoranas γ_2 and γ_3 together with the ancillary quantum dot, form an effective trijunction, with the coupling strengths being Γ_L, Γ_R and μ_D , respectively. Starting from uncoupled Majoranas with $\Gamma_L = \Gamma_R = 0$ and $\mu_D > 0$, we perform a sequence of three operations, adapting the protocol of Ref. [61]:

1. turn off μ_D while turn on Γ_L , $0 < t \leq T$
2. turn off Γ_L while turn on Γ_R , $T < t \leq 2T$
3. turn off Γ_R while turn on μ_D to its original value, $2T < t \leq 3T$.

The effect is to exchange the positions of γ_2 and γ_3 as shown in Fig. 1(c). The action of the braid protocol is described by the operator

$$B = U(3T) = \exp\left\{\frac{\pi}{4}\gamma_2\gamma_3\right\}. \quad (9)$$

Here we assume that all the operations are performed with perfect precision in the adiabatic limit and without any noise from the environment. The effect of the braiding operation becomes apparent when tracking the time

evolution of some initial state in the ground-state manifold through the time evolution. Due to fermion parity conservation in Eq. (1), we can focus on the subspace with total even parity without losing generality. When $\Gamma_L = \Gamma_R = 0$ and $\mu_D > 0$, the ground states are doubly degenerate with

$$\begin{aligned} |ee\rangle &\equiv \frac{1}{2}(|00\rangle_L - |11\rangle_L) \otimes (|00\rangle_R - |11\rangle_R) \otimes |0\rangle_D, \\ |oo\rangle &\equiv \frac{1}{2}(|10\rangle_L - |01\rangle_L) \otimes (|10\rangle_R - |01\rangle_R) \otimes |0\rangle_D, \end{aligned} \quad (10)$$

where the basis states are defined as $|n_{L1}, n_{L2}\rangle \otimes |n_{R1}, n_{R2}\rangle \otimes |n_D\rangle$. If the system is initialized as an even-even state

$$|\psi(0)\rangle = |ee\rangle, \quad (11)$$

it will evolve into

$$|\psi(3T)\rangle = B|\psi(0)\rangle = (|ee\rangle - i|oo\rangle)/\sqrt{2}, \quad (12)$$

after performing the braid operation once. By repeating the same braid operation, although Majoranas γ_2 and γ_3 return to their original positions, the system becomes

$$|\psi(6T)\rangle = B^2|\psi(0)\rangle = |oo\rangle, \quad (13)$$

which is orthogonal to the initial state. Equations (12) and (13) are regarded as the signatures of non-Abelian statistics of Majorana anyons. However, experimental demonstration of Eq. (12) would be challenging. What can be measured are probabilities $P_{|ee\rangle}(3T) = |\langle ee|\psi(3T)\rangle|^2$ and $P_{|oo\rangle}(3T) = |\langle oo|\psi(3T)\rangle|^2$, which do not contain the crucial information of the relative phase ($-i$) between the two basis states. Moreover, even a detection of $P_{|ee\rangle}(3T) = P_{|oo\rangle}(3T) = 1/2$, which is consistent with Eq. (12), cannot exclude the possibility of a completely decohered state with an uniform probability distribution. In contrast, measuring the outcome of a double braid operation in Eq. (13), which yields $P_{|ee\rangle}(6T) = 0$ and $P_{|oo\rangle}(6T) = 1$, will be transparent to interpret and thus more convincing. Therefore, in the rest of the work, we will focus on the double-braid protocol, which takes six steps of operations and a total time of $6T$, unless stated otherwise. A complete overview of the time-dependence of $P_{|oo\rangle}(t)$ is schematically shown in Fig. 1 (d).

C. Braiding in the imperfect case

A real system will deviate from this ideal case. For example, inter-dot Coulomb repulsion may lead to additional splittings, or some residual couplings between quantum dots may remain. Additionally, the "leg" of the effective trijunction formed by the middle quantum dot is not protected. Hence, noise in μ_D can be expected to

have a significant impact. Moreover, the phase-difference may deviate from the ideal value of π .

In the remainder of the paper, we will study the effects of these imperfections, and how to mitigate them. To this end, we will use the full Hamiltonian (1) with time-dependent parameters $\Gamma_{L/R}(t)$ and $\mu_D(t)$. We then compute $\psi(6T)$ by solving the time-dependent Schrödinger equation. For details on the simulations, we refer the reader to App. A.

To characterize the faithfulness of the protocol, we calculate the infidelity

$$1 - F \equiv 1 - |\langle oo|\psi(6T)\rangle|^2 = 1 - P_{|oo\rangle}(6T), \quad (14)$$

where $|\psi(6T)\rangle$ is the final state after time evolution through a double braid protocol and $|oo\rangle$ is the analytical target state, respectively. Note that the infidelity can be obtained experimentally from readout measurement on $P_{|ee\rangle}(6T)$ and $P_{|oo\rangle}(6T)$.

In our simulations, unless stated otherwise, we choose the system parameters to be $t_L = \Delta_L = t_R = \Delta_R = \Delta = 5\Gamma_0$, $\mu_{L1} = \mu_{L2} = \mu_{R1} = \mu_{R2} = 0$ to satisfy the sweet-spot condition, and $\varphi = \pi$ for the phase condition. Here, Γ_0 is the maximal strength of single electron tunneling setting the energy and time scale of the braiding process. We make sure that the time evolution satisfies the adiabatic limit, i.e. $T \gg h/\Gamma_0$, and assume no environmental noise or quasiparticle poisoning.

IV. INTERDOT COULOMB REPULSION

We now consider the effect of interdot Coulomb repulsion on Majorana braiding. Coulomb interaction is ubiquitous for quantum-dot-based devices, with the strength varying in a wide range of tens of μeV to as large as one meV [71, 72]. As described by H_C in Eq. (1), it is present among electrons on dots $L2, D$, and $R1$ due to the long-range nature of Coulomb interaction, while the interaction between dots within a Kitaev chain is strongly suppressed by the screening effect of the grounded superconductor.

We begin by assuming that Coulomb interaction is present, but that the three time-varying parameters have equal variation magnitude and can be tuned perfectly to zero,

$$0 \leq \Gamma_L(t), \Gamma_R(t), \mu_D(t) \leq \Gamma_0, \quad (15)$$

before relaxing this assumption in later discussions. As shown in Fig. 2 (a) ($U_L = U_R$) and (d) ($U_L \neq U_R$), interdot Coulomb energy has a very detrimental effect on braiding, with the infidelity quickly approaching one as $U \gtrsim \Gamma_0$.

To understand the physics behind this behavior, we focus on the first step of the braiding operation ($0 \leq t \leq T$). Since the right Kitaev chain is decoupled in this process, we can work on a simpler Hamiltonian of $H_{LD} =$

$H_{K,L} + H_{\text{tunn},L} + H_{C,L} + H_D$. Within the subspace of total even parity, it can be written as

$$H_{LD}^{(\text{even})} = \begin{pmatrix} 0 & -\frac{\Gamma_L}{2} & 0 & \frac{\Gamma_L}{2} \\ -\frac{\Gamma_L}{2} & \mu_D + \frac{U_L}{2} & \frac{\Gamma_L}{2} & -\frac{U_L}{2} \\ 0 & \frac{\Gamma_L}{2} & 2\Delta_L & \frac{\Gamma_L}{2} \\ \frac{\Gamma_L}{2} & -\frac{U_L}{2} & \frac{\Gamma_L}{2} & 2\Delta_L + \mu_D + \frac{U_L}{2} \end{pmatrix} \quad (16)$$

where the basis is $|e_L, 0_D\rangle, |o_L, 1_D\rangle, |e'_L, 0_D\rangle, |o'_L, 1_D\rangle$ and primes indicate excited states. Here we shift all states by Δ_L for simplicity of discussion, and the prime denotes the excited states in the Kitaev chain. In the tunneling regime of $\Gamma_L \ll \Delta_L$, the low-energy effective Hamiltonian is

$$H_{LD,\text{eff}}^{(\text{even})} = \begin{pmatrix} 0 & -\frac{\Gamma_L}{2}(a+b) \\ -\frac{\Gamma_L}{2}(a+b) & \mu_D + \frac{U_L}{2} + \Delta_L - \lambda \end{pmatrix} \quad (17)$$

for arbitrary strength of U_L , and valid up to second order in Γ_L . Here $\lambda = \sqrt{\Delta_L^2 + (U_L/2)^2}$, and a, b are positive numbers with $a^2 = 1 - b^2 = \frac{1}{2} + \frac{\Delta_L}{2\lambda}$. The low-energy basis states are $|\psi_1\rangle = |e_L, 0_D\rangle$, and $|\psi_2\rangle = a|o_L, 1_D\rangle + b|o'_L, 1_D\rangle$. There are two major effects from the interdot Coulomb repulsion. First, the instantaneous ground state of the total system now includes a component of the excited states $|o'_L\rangle$ in $|\psi_2\rangle$, compared to the idealized $|\psi_2\rangle = |o_L, 1_D\rangle$ for the case with $U_L = 0$. Second, as shown in Eq. (17), the effective energy of the ancillary quantum dot is shifted: $\mu_D \rightarrow \mu_D + \frac{U_L}{2} + \Delta_L - \lambda$, which enhances the energy of $|\psi_2\rangle$. In the strong Coulomb regime, $0 \leq \mu_D \leq \Gamma_0$ does not effectively take the dot down to resonance, and as a result, the system would stay close to $|ee\rangle$ without moving any Majoranas, which explains the high infidelity in Fig. 2(a). Based on Eq. (17), one way to mitigate this detrimental error is to shift the dot energy as below

$$\begin{aligned} \mu_{D,\text{min}} &\leq \mu_D(t) \leq \mu_{D,\text{min}} + \Gamma_0, \\ \mu_{D,\text{min}} &= \mu_D^* = \sum_{a=L,R} \left(-\frac{U_a}{2} - \Delta_a + \sqrt{\Delta_a^2 + (U_a/2)^2} \right). \end{aligned} \quad (18)$$

Note that the dot energy shift now includes contributions from both Kitaev chains because the Coulomb potential is additive and we assume no coupling between the two Kitaev chains directly. Applying Eq. (18) to the braid protocol and without changing any other conditions, we obtain the blue curve in Fig. 2 (a) for $U_L = U_R$ and (d) for $U_L \neq U_R$. It shows an excellent correction of the errors with $1 - F \lesssim 10^{-3}$, validating our analysis and proposal. Notably, since our treatment of Coulomb repulsion is nonperturbative in the interaction strength, the error mitigation applies to strong Coulomb case ($U > \Delta$) as well, provided the system stays in the tunneling regime $\Gamma_L \ll \Delta_L$. Figure 2 (a) and (d) are the first main findings of this work, which positively indicates that it is possible to mitigate the detrimental effect of interdot Coulomb repulsion in Majorana braiding.

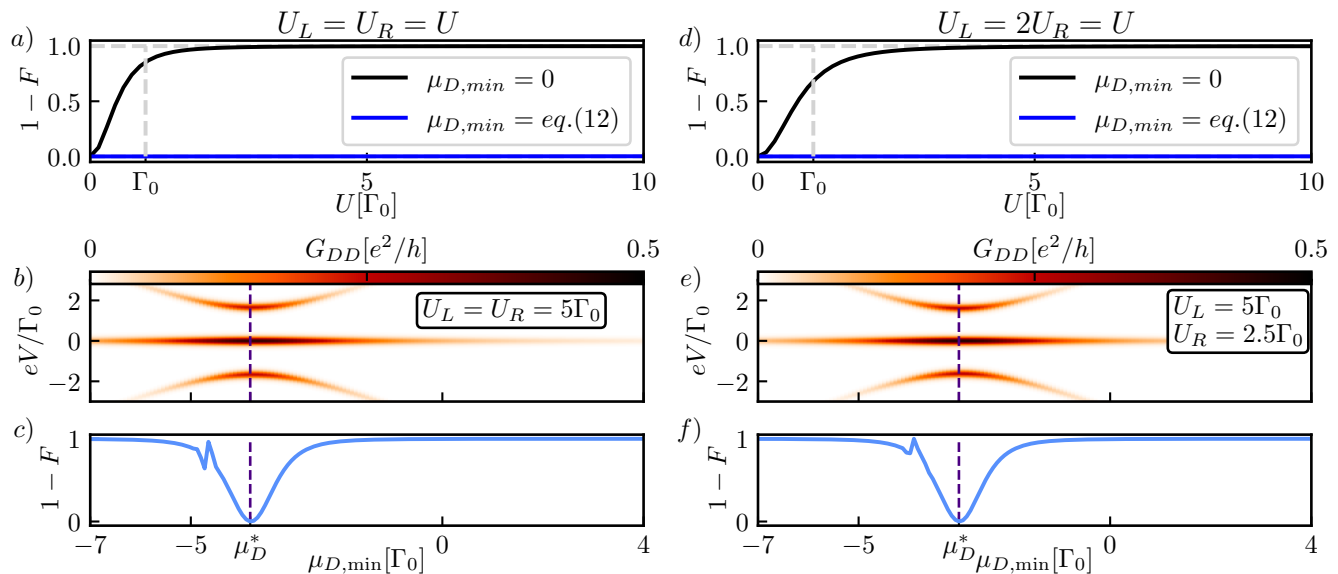


FIG. 2. Effects of interdot Coulomb interaction between ancillary dot and adjacent Kitaev chain dots. (a) and (d) show the infidelity in dependence of symmetric and asymmetric Coulomb energy respectively. (b) and (e) show local conductance spectroscopy through the ancillary dot. Due to the interaction, the excitation minimum shifts in chemical potential to a lower value corresponding to Eq. (18). Retuning $\mu_{D,\min}$ to this value corrects the adverse effect of the Coulomb interaction. This is supported by (c) and (f) showing the infidelity in dependence of $\mu_{D,\min}$. In line with the excitation minimum, the infidelity reduces to zero when $\mu_{D,\min} = \mu_D^*$. The discontinuity at $\mu_D^* - \Gamma_0$ is due to our choice of $\mu_{D,\max} - \mu_{D,\min} = \Gamma_0$ where the occupied state on the dot becomes resonant with the states in the Kitaev chains. Measuring the traces as those presented in (c) and (f) experimentally can be considered a signature of Majorana braiding.

To find the value of μ_D^* in an actual device, we propose two experiments. The first one is a local tunnel spectroscopy on the ancillary dot in the (eV, μ_D) plane, as shown in Fig. 2(b) and (e). Here a normal lead is coupled to the ancillary dot to obtain G_{DD} . Although the Majorana-induced zero-bias peak stays robust, the subgap peak from the first excited state varies with μ_D , and reaches a minimum along the bias-voltage axis at $\mu_D = \mu_D^*$ [see Fig. 2(b) and (e)], thus providing a way to find μ_D^* for the braid protocol. Note that this does not add to the device complexity, when transport measurements are needed to fine-tune the Kitaev chains into their sweet spots. Our second proposal is to measure the infidelity as a function of $\mu_{D,\min}$. As shown in Fig. 2(c) and (f), the infidelity drops to nearly zero at the optimal value $\mu_{D,\min} = \mu_D^*$, and then increases to one when $\mu_{D,\min}$ is tuned away by $\sim \Gamma_0$. The numerical simulations are consistent with our analytical results in Eq. (17) and (18). Moreover, a measurement of Figs. 2(c) or 2(f) can be regarded as a signature of successful Majorana braiding. We note that the apparent discontinuity visible in Fig. 2 (c) and (f) are a consequence of our initial choice $\max(\mu_D(t)) = \Gamma_0$. When $\mu_{D,\min} \rightarrow \mu_D^* - \Gamma_0$ the occupied state of the ancillary dot is on resonance with the states on the Kitaev chain, interfering with the braiding. As this happens only for $\mu_{D,\min} < \mu_D^*$ and can be controlled by changing $\max(\mu_D(t)) > \Gamma_0$, this feature can be disregarded for the effectiveness of the central result

at μ_D^* .

V. RESIDUAL SINGLE ELECTRON TUNNELING

In semiconducting quantum dot devices, the single electron tunneling strength is controlled by electrostatic gates. Although the strength can be varied deterministically, it is challenging to turn off the coupling completely, causing unwanted errors in qubit control [73, 74]. To study the effect of residual coupling we assume

$$\Gamma_{\min} \leq \Gamma_L(t), \Gamma_R(t) \leq \Gamma_0, \quad (19)$$

$$\mu_{D,\min} \leq \mu_D(t) \leq \mu_{D,\min} + \Delta\mu_D, \quad (20)$$

where $\Gamma_{\min} > 0$ is the residual tunneling strength, and $\Delta\mu_D = \mu_{D,\max} - \mu_{D,\min}$ is the variation magnitude of the ancillary dot energy. For the analytic considerations we set the interdot Coulomb energy at first to zero, unless stated otherwise (we relax this assumption in Fig. 4 (c) and (d)). Figure 3(a) shows the numerically calculated infidelities in the $(\Delta\mu_D, \Gamma_{\min})$ plane. The infidelity increases with the residual tunneling strength Γ_{\min} while it decreases with the dot variation magnitude $\Delta\mu_D$, see Figs. 3(b) and 3(c). As it will be shown below, the infidelity is a joint consequence of two distinct error mechanisms, which we call leakage and geometrical leakage error.

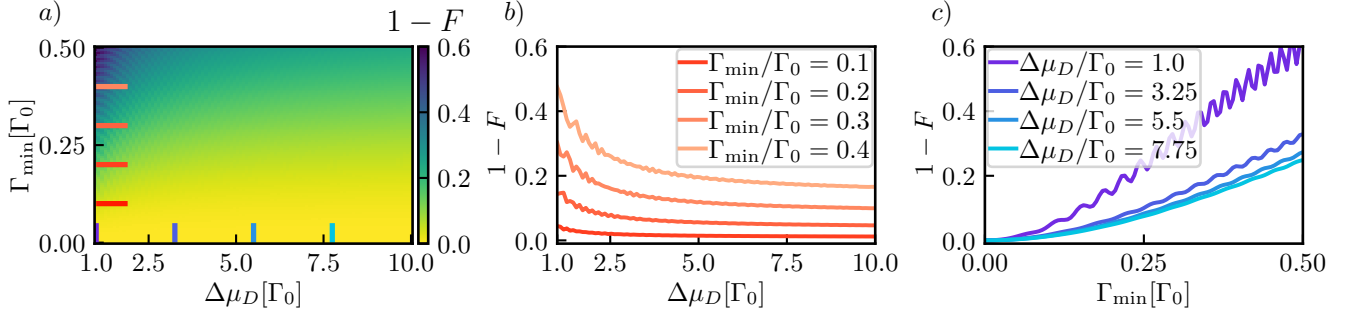


FIG. 3. (a) Infidelity, $1 - F$, in the $(\Delta\mu_D, \Gamma_{\min})$ -plane. (b) Infidelity as a function of $\Delta\mu_D$ for different cuts of Γ_{\min} in (a). (c) Infidelity as a function of Γ_{\min} for different cuts of $\Delta\mu_D$ in (a).

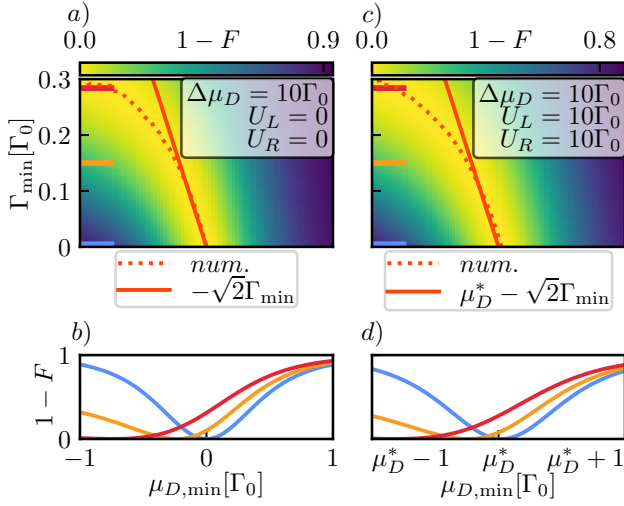


FIG. 4. (a) and (c) Infidelity, $1 - F$, in the $(\mu_{D,\min}, \Gamma_{\min})$ plane for $U_a = 0$ and $U_a = 10\Gamma_0$ respectively. For both, we choose $\Delta\mu_D = 10\Gamma_0$. The dotted lines show the numerical minimum of the infidelity, solid lines correspond to the expectation of eqns. (30) and (18). (b) and (d) Infidelity as a function of $\mu_{D,\min}$ for different cuts in Γ_{\min} through (a) and (c) showing that for increasingly negative values of $\mu_{D,\min}$ the infidelity vanishes regardless of residual tunnel coupling.

The leakage error, on one hand, can be understood from a heuristic perturbation theory analysis: At the initial time, treating the residual tunnelings $\Gamma_{a,\min}$ as a perturbative effect, the state $|ee\rangle$ can leak into the excited states

$$|oe\rangle = \frac{1}{2}(|10\rangle_L - |01\rangle_L) \otimes (|00\rangle_R - |11\rangle_R) \otimes |1\rangle_D \quad (21)$$

$$|eo\rangle = \frac{1}{2}(|00\rangle_L - |11\rangle_L) \otimes (|10\rangle_R - |01\rangle_R) \otimes |1\rangle_D \quad (22)$$

with a characteristic amplitude of $\Gamma_{\min}/\Delta\mu_D$. Thus the leakage probability is

$$P_{\text{leak}} \propto \left(\frac{\Gamma_{\min}}{\Delta\mu_D} \right)^2 \quad (23)$$

to leading order in residual tunneling strength. The same argument can be made for any specific state expected at an intermediate step of the time evolution. In light of Eq. (14), for a perfect double braid besides residual couplings of the Majoranas, it is therefore to expect that $1 - F = 1 - P_{|oo\rangle} \propto P_{\text{leak}} \times \text{const.}$, with a constant proportional to T . Indeed, as shown in Fig. 3(c), the numerically calculated infidelity decays with a larger variation magnitude, consistent with Eq. (23). As indicated by Eq. (23), leakage errors can be mitigated by an increase of the chemical potential variation on the ancillary dot, i.e.

$$\Delta\mu_D \gg \Gamma_0. \quad (24)$$

We note that an increase of $\Delta\mu_D$ comes at the expense of diabatic errors due to faster changes of $\mu_D(t)$. We do however expect the existence of a window in protocol time where the leakage error is strongly suppressed before the diabatic error becomes prominent.

The geometrical error, on the other hand, can be understood by calculating the unitary evolution operator, Eq. (9), in the presence of residual couplings between the Majoranas. This amounts to calculating the non-Abelian Berry phase of the cyclic variation of the Hamiltonian, which has a geometrical origin. Performing a similar calculation to that of Ref. [61] generalized to asymmetric couplings (see App. C), the unitary operator in Eq. (9) becomes

$$U_{\text{res}}(3T) = \exp \left\{ \left(\frac{\pi}{4} - \epsilon \right) \gamma_2 \gamma_3 \right\}, \quad (25)$$

where ϵ denotes the deviation from perfect braiding. The corresponding infidelity is

$$1 - F = \sin^2(2\epsilon) \approx 4\epsilon^2 \quad (26)$$

when $\epsilon \ll 1$. Calculating ϵ in Eq. (25) explicitly, we find for $\Gamma_{L,\max} = \Gamma_{R,\max} = \mu_{D,\max} = \Gamma_0$

$$\epsilon \approx \frac{1}{\sqrt{2}\Gamma_0} (\Gamma_{L,\min} + \Gamma_{R,\min} + \mu_{D,\min}) \quad (27)$$

in leading order of the residual coupling of the Majoranas (see App. C). We note that Eq. (27) coincides with the result in Ref. [61] when $\Gamma_{L,\min} = \Gamma_{R,\min} = \mu_{D,\min}$. Assuming no residual coupling of the Majoranas on the ancillary dot, i.e. $\mu_{D,\min} \equiv 0$ in the absence of Coulomb repulsion, we find through Eq. (26) that the infidelity scales quadratically with the residual tunnel coupling,

$$1 - F \propto \left(\frac{\Gamma_{\min}}{\Gamma_0} \right)^2. \quad (28)$$

We can find an analytical correction to the geometrical error when excluding the presence of leakage errors, that is in the limit $\Gamma_{L,\max} = \Gamma_{R,\max} = \Gamma_0 \ll \mu_{D,\max}$. We then obtain

$$\epsilon \approx \frac{1}{\sqrt{2}\Gamma_0} \left(\Gamma_{L,\min} + \Gamma_{R,\min} + \sqrt{2}\mu_{D,\min} \right), \quad (29)$$

to leading order in residual tunnelings and in $\Gamma_0/\mu_{D,\max}$. The key observation now is that, despite $\Gamma_{a,\min}/\Gamma_{a,\max} > 0$ for any applied voltage to the tunnel gates, one can change the sign of $\mu_{D,\min}$ with respect to $\mu_{D,\max}$ by tuning the dot to chemical potentials below the resonance of dot with the Kitaev chains. In particular, the geometrical error vanishes up to the leading (quadratic) order in Γ_{\min}/Γ_0 when one chooses

$$\mu_{D,\min} = -\sqrt{2}\Gamma_{\min} < 0. \quad (30)$$

Figure 4 (a) shows the infidelity of the double braid protocol in the $(\mu_{D,\min}, \Gamma_{\min})$ plane for $\Delta\mu_D = 10\Gamma_0$. The dotted red line indicates the numerical minimum of the infidelity, $1 - F$, for fixed Γ_{\min} in dependence of $\mu_{D,\min}$ while the solid red line shows Eq.(30). Indeed, the optimized $\mu_{D,\min}$ take negative values as predicted. Moreover, the analytic result in Eq. (30) matches well with the numerical result in the weak residual tunneling regime. We furthermore find that our analysis remains well valid even in the presence of Coulomb repulsion when additionally applying the correction suggested in Sec. IV, i.e. $\mu_D \rightarrow \mu_D + \mu_D^*$ as visible in Fig. 4 (c) and (d).

VI. SUPERCONDUCTING PHASE DIFFERENCE

Satisfying the phase condition $\varphi = \pi$ is crucial for a successful braiding experiment. The phase is controlled via the magnetic flux through the superconducting loop, i.e. $\varphi = 2\pi e\Phi/h + \text{const.}$, see Fig. 1(a). Here we propose two experiments to find where $\varphi = \pi$, which are similar in spirit to those discussed in Sec. IV. The first one is a transport measurement. Figure 5(a) shows the tunnel spectroscopy of G_{DD} in the (eV, φ) plane. The signature of $\varphi = \pi$ is a zero-bias conductance peak, which is induced by the Majorana zero modes formed at the trijunction and splits linearly when the phase is away

from π . Our second proposed experiment is to measure the double-braid infidelity $1 - F$ as a function of φ , as shown in Fig. 5(b). Interestingly, in addition to $\varphi = \pi$, there are multiple other values of φ also giving zeros of $1 - F$. These zeros are due to Rabi oscillations induced by the undesired ground-state degeneracy splitting, similar to the observations in Ref. [68, 75]. However, a fundamental distinction between them is that the outcome of non-Abelian braiding does not depend on the precise control of the protocol time as the dynamical effects such as Rabi oscillations. Therefore, after averaging over different lengths of protocol time T , while keeping the adiabaticity constraint still satisfied, only the infidelity at $\varphi = \pi$ remains zero [see Fig. 7(c)], indicating the robustness of a geometrical braid operation.

In addition, we notice that both the conductance spectroscopy and the infidelities in Fig. 5 are 2π -periodic in φ , or equivalently $h/2e$ -periodic in magnetic flux Φ . However, the tunneling Γ_R in Eq. (1) at $\varphi = 3\pi$ acquires a minus sign relative to $\varphi = \pi$, giving

$$B_{3\pi} = B_{\pi}^{-1}, \quad (31)$$

where B_{π} is defined in Eq. (9). This is a consequence of the 4π Josephson effect due to fractionalized Majorana zero modes. In particular, single braids B_{π} and $B_{3\pi}$ give $(|ee\rangle \pm i|oo\rangle)/\sqrt{2}$, respectively. However, it is challenging to distinguish the different phases $\pm i$ here from a measurement of $P_{|ee\rangle}$ and $P_{|oo\rangle}$ only. Thus we propose the following three-step experiment.

1. apply B_{π} on $|ee\rangle$ twice to obtain $|oo\rangle$
2. apply $B_{3\pi}$ on $|ee\rangle$ twice to obtain $|oo\rangle$
3. apply B_{π} on $|ee\rangle$ once followed by another $B_{3\pi}$ to obtain $|ee\rangle$

Here in each step the system should be initialized at $|ee\rangle$. A successful implementation of the above experiments would manifest 4π -periodicity in a fractional Josephson junction. We demonstrate our proposal in Fig. 5 for the system described in Sec. III C for $\Delta\mu_D = 1$ and without Coulomb repulsion. We see that, if the phase stays constant over the double braid, the Majoranas exchange as expected and the quantum state of the system changes. If, however, the phase is adiabatically changed for the second exchange the state returns to the initial state due to the 4π -Josephson effect.

VII. DIABATIC AND DEPHASING EFFECTS

We now consider the impact of diabatic and dephasing errors when executing the braid protocol. Figure 7 shows the infidelity as a function of the protocol step time T at time $t = 6T$ for different values of $\Delta\mu_D$ and U . The infidelity decreases exponentially with the protocol time, consistent with the behavior of diabatic error in holonomy or anyonic braiding [76]. Interestingly, by

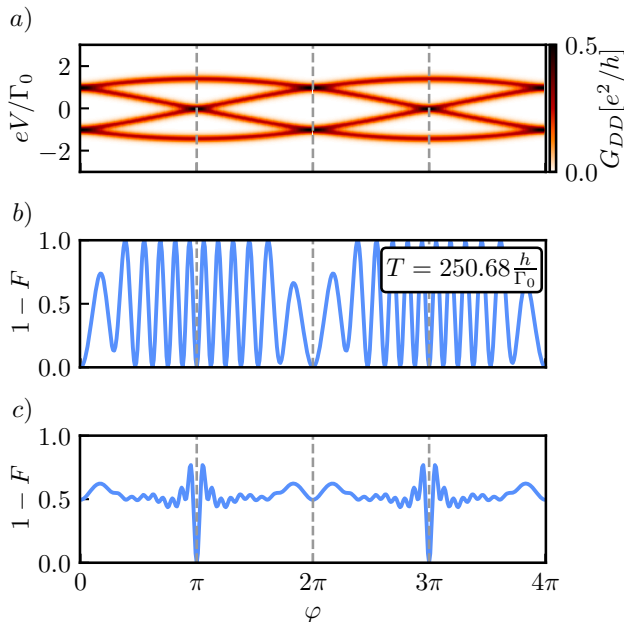


FIG. 5. (a) Tunnel spectroscopy, G_{DD} , over the ancillary dot in the (V, φ) plane. Only at odd integer multiples of π the conductance indicates the necessary degeneracy at $V = 0$. Additionally, the linear splitting of that degeneracy with phase indicates the lack of protection of the protocol against phase noise. (b) Infidelity, $1 - F$, as a function of φ for a single T . The oscillations indicate Rabi oscillations between the states in the ground-state manifold. (c) Infidelity of the double braid protocol averaged over multiple T . Since the outcome of the non-Abelian exchange does not depend on any specific choice of T , the perfect fidelities at odd interger multiples of π persist while the Rabi oscillations present in (b) average away.

comparing the blue and orange lines in Fig. 7(a), we find that increasing $\Delta\mu_D$ decreases the diabatic error. Physically, although the change of $\mu_D(t)$ becomes faster, the energy gap of the effective trijunction increases, which compensates the former effect as long no Landau-Zener transitions into the excited manifold are induced. This means that we can suppress the leakage in Eq. (23) without increasing the diabatic error. Additionally, with finite Coulomb, the infidelity saturates at $1 - F \approx 10^{-3}$ for $T \rightarrow \infty$, which is due to the higher-order corrections to μ_D^* from Γ_a that are not included in leading-order result shown in Eq. (18).

In semiconducting quantum dot devices, charge noise is the primary source of noise, which can be caused by charge impurities or gate voltage fluctuations [77–84]. Since it is $1/f$ noise, which is dominated by the low-frequency component, we can model the noises using the quasi-static disorder approximation [85, 86]. In particular, we focus on the effect of noise in the ancillary dot that does not exhibit any protection, whereas noise in the short Kitaev chains could be mitigated by extending the chain length. Moreover, the dephasing effects of noise

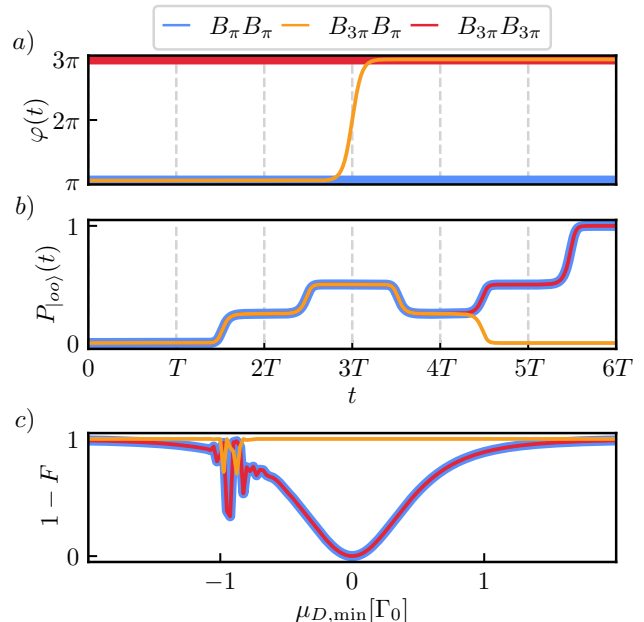


FIG. 6. Time and dot chemical potential traces demonstrating the 4π -Josephson effect of the system for the system specified in Sec. III C up to phase. We choose $\Delta\mu_D = 1$ and neglect interdot Coulomb repulsion. (a) Superconducting phase φ in dependence of time. To implement $B_\pi B_\pi$ and $B_{3\pi} B_{3\pi}$ we keep the phase fixed while for $B_{3\pi} B_\pi$ we adiabatically change the phase from $\pi \rightarrow 3\pi$ around $t = 3T$. (b) occupation probability of the $|oo\rangle$ state. Only for $B_{3\pi} B_\pi$, the initialized $|ee\rangle$ state returns into itself over the time evolution. (c) Infidelity, $1 - F$, depending on $\mu_{D,\min}$. Only the $B_\pi B_\pi$ and $B_{3\pi} B_{3\pi}$ show the transition from $|ee\rangle \rightarrow |oo\rangle$ predicted for non-Abelian exchange. For $B_{3\pi} B_\pi$ the initial state returns to itself identically.

within the Kitaev chains were studied in previous work in the context of imperfect Majorana polarizations [59].

We assume the noise on the ancillary dot chemical potential can be modeled as

$$\mu_D(t) \rightarrow \mu_D(t) + \delta\mu_D, \quad (32)$$

where $\delta\mu_D$ is a constant shift drawn from a normal distribution with width σ_{μ_D} and centered around zero for each execution of the protocol (see App. A). To quantify the effect of the noise we perform an ensemble average over 100 different noise values. As shown in Fig. 7(b), the main effect of μ_D -noise is to deteriorate the fidelity around $\mu_{D,\min} = \mu_D^*$ ($= 0$ when $U_a = 0$). Since the width of the $1 - F$ dip is of the order of Γ_0 , a necessary condition for observing this signature is a characteristic disorder strength $\mu_{D,\text{dis}} \ll \Gamma_0$ to indicate the success of the braid.

In contrast to chemical potential noise, the modeling of the tunneling noise, Γ , differs due to its distinct dependence on the electrostatic potential. In particular, the quantum dot energy has a linear dependence because it is capacitively coupled to the electrostatic potential

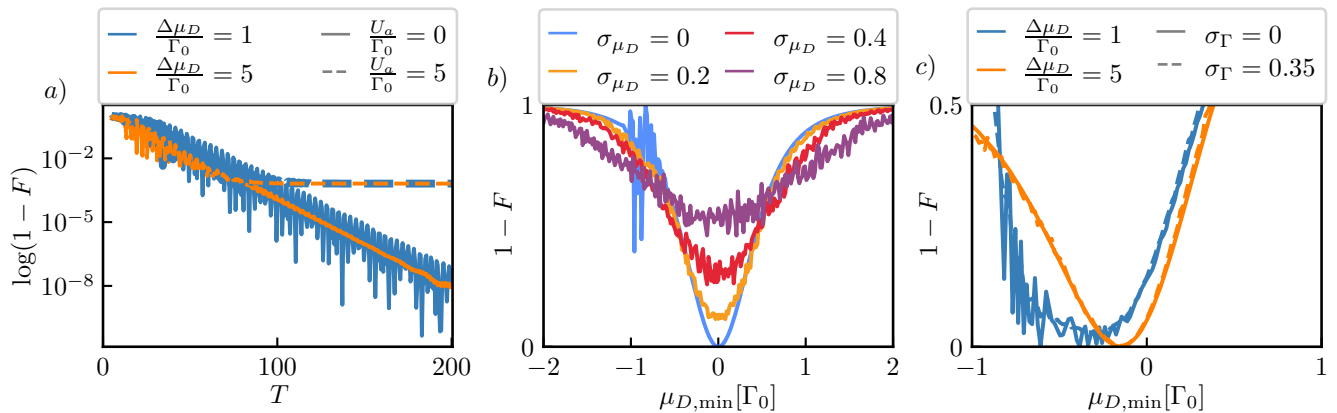


FIG. 7. (a) Logarithm of the infidelity, $\log 1 - F$, in dependence of protocol step time T showing oscillations due to leakage into excited states. The reduced fidelity at finite U is due to perturbative corrections to μ_D^* Γ_a not taken into account in Eq. (18). (b) Ensemble averaged infidelity of the double braid in dependence of $\mu_{D,\min}$ for different variances of quasistatic noise on μ_D averaged over 100 realizations. (c) Ensemble averaged infidelity in dependence of $\mu_{D,\min}$ at fixed residual tunneling $\Gamma_{\min} = 0$ over 100 noise values. Solid and dashed lines correspond to noise with a variance of 0 and $0.35\Gamma_0$ on the tunnel coupling Γ_a respectively.

nearby, while the electron transfer rate has an exponential dependence since it is determined by the transmission probability through a tunnel barrier. Therefore, noise in Γ_a is proportional to Γ_a itself, i.e.

$$\Gamma_a(t) \rightarrow (1 + \alpha) \Gamma_a(t), \quad (33)$$

Here α is a dimensionless coefficient which we draw from a normal distribution of width σ_Γ and mean zero. We use this simple model of noise on tunneling, as it avoids taking into account details of the tunnel barrier, but we expect it is sufficient to demonstrate the principal effect of noise in the tunnel barriers when ensuring $\sigma_\Gamma \ll 1$. As shown in Fig. 7(c), although the $1 - F$ dip is again lifted by the noise, its effect is much weaker to the effect of chemical potential noise as shown in Fig. 7(b). This feature can be well understood using Eq. (33). When the tunneling Γ_a is in the *off*-state, the fluctuation is strongly suppressed due to the small residual tunneling amplitude. On the other hand, the deviation of Γ_a strength in the *on*-state predominantly changes the energy gap of the effective trijunction, without greatly affecting the outcome braiding operation. Thus, tunneling noise is less detrimental than noise on μ_D in this braid setup.

VIII. DISCUSSION

It has been shown that braiding of non-Abelian anyons can take place only in two-dimensional space, which seemingly contradicts with the conclusions of the current work. However, we emphasize that although the quantum dot-superconductor array has a linear structure at the first glance, it is quasi-one-dimensional in nature. In particular, since $\varphi = \pi$ is a crucial requirement for a successful Majorana braid, a superconducting loop [see

Fig. 1(a)] has to be formed along with a controllable magnetic flux Φ , which extends the setup geometry to the second dimension. Moreover, the proposed braiding setup allows a "minimal braiding" experiment in the sense that the outcome is *not* topologically protected, but depends on fine-tuning of parameters, in particular μ_D and ϕ .

We here discuss several relevant time scales of the braiding protocol. First, the protocol time should be sufficiently long in order to satisfy the adiabatic condition. Although there is no common standard, here we choose a threshold diabatic error to be 10^{-2} for concrete discussions. According to Fig. 7(a), the protocol time needs to be larger than $\sim 300\hbar/\Gamma_0$, which corresponds to a time scale of ~ 20 ns for a typical single electron tunneling strength of $\Gamma_0 \sim 10 \mu\text{eV}$.

Second, as discussed in Sec. VII, the dephasing effect from noises in μ_D and those within Kitaev chains should be sufficiently mitigated. In particular, in order to experimentally observe Fig. 2(c) or (f), which is regarded as one of the signatures of a successful Majorana braiding, the amplitude of the μ_D noise must be smaller than the characteristic single electron tunneling strength, i.e.,

$$\mu_{D,\text{dis}} \ll \Gamma_0, \quad (34)$$

as shown in Fig. 7(b). Additionally, the energy splitting between the instantaneous ground states should also be much weaker than Γ_0 to avoid decoherence. This can be achieved by either enhancing the excitation gap of a Kitaev chain [27, 28, 33] or extending the chain length [30, 31, 40, 43]. By contrast, based on our simulations and arguments, the noises in $\Gamma_{L/R}$ are less detrimental.

The third time scale is the quasiparticle poisoning effect. For example, a random incoming electron from out-

side the system can flip the total fermion parity, causing leakage errors that cannot be corrected. The poisoning time is reported to be around ~ 1 ms in devices of InSb/InAs semiconductor nanowires proximitized by Al superconductors [87], which has a very similar nanostructure to the Kitaev chain devices [26–31]. As long as the adiabatic condition is satisfied (e.g., ~ 20 ns for diabatic error $< 10^{-2}$) within that time scale, the quasiparticle poisoning effect should not be a major concern in this braid experiment.

IX. SUMMARY

In summary, we have investigated a minimal Majorana braiding protocol in quantum-dot-based Kitaev chains, focusing on the physical phenomena that are peculiar to quantum dot devices, e.g., interdot Coulomb repulsion and residual single electron tunneling. We find that the detrimental errors from them can be efficiently mitigated by optimal control of the ancillary quantum dot

via $\mu_{D,\min}$ and $\mu_{D,\max}$. Furthermore, we propose a series of experiments to find this optimal operating regime and predict signatures of a successful braiding. We also analyze the diabatic errors and dephasing effect from various types of noises.

Author contributions C.X.L., F.Z., and M.W. initiated the project. C.X.L. and S.M. designed the project. S.M. and C.X.L. performed the calculations with input from A.M.B.. C.X.L. supervised the project with input from M.W.. S.M., C.X.L., and M.W. wrote the manuscript with input from all authors.

Acknowledgements We acknowledge useful discussions with Alberto Bordin, Bart Roovers, Florian Bennebroek Evertsz, and Juan Daniel Torres Luna about current experiments and their analysis. This work was supported by a subsidy for top consortia for knowledge and innovation (TKI toeslag), by the Dutch Organization for Scientific Research (NWO) and Microsoft Station Q. S.M. acknowledges funding of NWO through OCENW.GROOT.2019.004.

Data availability The code and the data that was generated for the plots are available in the repository of Ref. [88]

-
- [1] G. Moore and N. Read, Nonabelions in the fractional quantum hall effect, *Nuclear Physics B* **360**, 362 (1991).
 - [2] C. Nayak, S. H. Simon, A. Stern, M. Freedman, and S. Das Sarma, Non-Abelian anyons and topological quantum computation, *Rev. Mod. Phys.* **80**, 1083 (2008).
 - [3] S. D. Sarma, M. Freedman, and C. Nayak, Majorana zero modes and topological quantum computation, *Npj Quantum Information* **1**, 15001 EP (2015).
 - [4] J. Alicea, New directions in the pursuit of Majorana fermions in solid state systems, *Rep. Prog. Phys.* **75**, 076501 (2012).
 - [5] M. Leijnse and K. Flensberg, Introduction to topological superconductivity and Majorana fermions, *Semicond. Sci. Technol.* **27**, 124003 (2012).
 - [6] C. Beenakker, Search for Majorana fermions in superconductors, *Annu. Rev. Condens. Matter Phys.* **4**, 113 (2013).
 - [7] T. D. Stanescu and S. Tewari, Majorana fermions in semiconductor nanowires: fundamentals, modeling, and experiment, *J. Phys.: Condens. Matter* **25**, 233201 (2013).
 - [8] J.-H. Jiang and S. Wu, Non-Abelian topological superconductors from topological semimetals and related systems under the superconducting proximity effect, *J. Phys.: Condens. Matter* **25**, 055701 (2013).
 - [9] S. R. Elliott and M. Franz, Colloquium: Majorana fermions in nuclear, particle, and solid-state physics, *Rev. Mod. Phys.* **87**, 137 (2015).
 - [10] M. Sato and Y. Ando, Topological superconductors: a review, *Rep. Prog. Phys.* **80**, 076501 (2017).
 - [11] R. Aguado, Majorana quasiparticles in condensed matter, *La Rivista del Nuovo Cimento* **40**, 523 (2017).
 - [12] R. M. Lutchyn, E. P. A. M. Bakkers, L. P. Kouwenhoven, P. Krogstrup, C. M. Marcus, and Y. Oreg, Majorana zero modes in superconductor–semiconductor heterostructures, *Nat. Rev. Mater.* **3**, 52 (2018).
 - [13] H. Zhang, D. E. Liu, M. Wimmer, and L. P. Kouwenhoven, Next steps of quantum transport in Majorana nanowire devices, *Nat. Commun.* **10**, 5128 (2019).
 - [14] E. Prada, P. San-Jose, M. W. A. de Moor, A. Geresdi, E. J. H. Lee, J. Klinovaja, D. Loss, J. Nygård, R. Aguado, and L. P. Kouwenhoven, From andreev to majorana bound states in hybrid superconductor–semiconductor nanowires, *Nature Reviews Physics* **2**, 575 (2020).
 - [15] L. Fu and C. L. Kane, Superconducting proximity effect and majorana fermions at the surface of a topological insulator, *Phys. Rev. Lett.* **100**, 096407 (2008).
 - [16] J. D. Sau, R. M. Lutchyn, S. Tewari, and S. Das Sarma, Generic new platform for topological quantum computation using semiconductor heterostructures, *Phys. Rev. Lett.* **104**, 040502 (2010).
 - [17] R. M. Lutchyn, J. D. Sau, and S. Das Sarma, Majorana fermions and a topological phase transition in semiconductor–superconductor heterostructures, *Phys. Rev. Lett.* **105**, 077001 (2010).
 - [18] Y. Oreg, G. Refael, and F. von Oppen, Helical liquids and Majorana bound states in quantum wires, *Phys. Rev. Lett.* **105**, 177002 (2010).
 - [19] J. D. Sau and S. D. Sarma, Realizing a robust practical Majorana chain in a quantum-dot–superconductor linear array, *Nat. Commun.* **3**, 964 (2012).
 - [20] J. Liu, A. C. Potter, K. T. Law, and P. A. Lee, Zero-bias peaks in the tunneling conductance of spin-orbit-coupled superconducting wires with and without majorana end-states, *Phys. Rev. Lett.* **109**, 267002 (2012).
 - [21] S. Mi, D. Pikulin, M. Marciiani, and C. Beenakker, X-shaped and y-shaped andreev resonance profiles in a superconducting quantum dot, *JETP* **119**, 1018 (2014).
 - [22] H. Pan and S. Das Sarma, Physical mechanisms for zero-

- bias conductance peaks in majorana nanowires, *Phys. Rev. Res.* **2**, 013377 (2020).
- [23] C.-X. Liu, G. Wang, T. Dvir, and M. Wimmer, Tunable superconducting coupling of quantum dots via andreev bound states in semiconductor-superconductor nanowires, *Phys. Rev. Lett.* **129**, 267701 (2022).
- [24] A. Bordin, G. Wang, C.-X. Liu, S. L. D. ten Haaf, N. van Loo, G. P. Mazur, D. Xu, D. van Driel, F. Zatelli, S. Gazibegovic, G. Badawy, E. P. A. M. Bakkers, M. Wimmer, L. P. Kouwenhoven, and T. Dvir, Tunable crossed andreev reflection and elastic cotunneling in hybrid nanowires, *Phys. Rev. X* **13**, 031031 (2023).
- [25] M. Leijnse and K. Flensberg, Parity qubits and poor man's Majorana bound states in double quantum dots, *Phys. Rev. B* **86**, 134528 (2012).
- [26] T. Dvir, G. Wang, N. van Loo, C.-X. Liu, G. P. Mazur, A. Bordin, S. L. D. ten Haaf, J.-Y. Wang, D. van Driel, F. Zatelli, X. Li, F. K. Malinowski, S. Gazibegovic, G. Badawy, E. P. A. M. Bakkers, M. Wimmer, and L. P. Kouwenhoven, Realization of a minimal kitaev chain in coupled quantum dots, *Nature* **614**, 445 (2023).
- [27] S. L. D. ten Haaf, Q. Wang, A. M. Bozkurt, C.-X. Liu, I. Kulesh, P. Kim, D. Xiao, C. Thomas, M. J. Manfra, T. Dvir, M. Wimmer, and S. Goswami, A two-site kitaev chain in a two-dimensional electron gas, *Nature* **630**, 329 (2024).
- [28] F. Zatelli, D. van Driel, D. Xu, G. Wang, C.-X. Liu, A. Bordin, B. Roovers, G. P. Mazur, N. van Loo, J. C. Wolff, A. M. Bozkurt, G. Badawy, S. Gazibegovic, E. P. A. M. Bakkers, M. Wimmer, L. P. Kouwenhoven, and T. Dvir, Robust poor man's majorana zero modes using yu-shiba-rusinov states, *Nat. Commun.* **15**, 7933 (2024).
- [29] A. Bordin, X. Li, D. van Driel, J. C. Wolff, Q. Wang, S. L. D. ten Haaf, G. Wang, N. van Loo, L. P. Kouwenhoven, and T. Dvir, Crossed andreev reflection and elastic cotunneling in three quantum dots coupled by superconductors, *Phys. Rev. Lett.* **132**, 056602 (2024).
- [30] A. Bordin, C.-X. Liu, T. Dvir, F. Zatelli, S. L. ten Haaf, D. van Driel, G. Wang, N. van Loo, T. van Caekenberghe, J. C. Wolff, *et al.*, Signatures of majorana protection in a three-site kitaev chain, [arXiv:2402.19382](https://arxiv.org/abs/2402.19382) (2024).
- [31] S. L. ten Haaf, Y. Zhang, Q. Wang, A. Bordin, C.-X. Liu, I. Kulesh, V. P. Sietses, C. G. Prosko, D. Xiao, C. Thomas, *et al.*, Edge and bulk states in a three-site kitaev chain, [arXiv:2410.00658](https://arxiv.org/abs/2410.00658) (2024).
- [32] A. Tsintzis, R. S. Souto, and M. Leijnse, Creating and detecting poor man's majorana bound states in interacting quantum dots, *Phys. Rev. B* **106**, L201404 (2022).
- [33] C.-X. Liu, A. M. Bozkurt, F. Zatelli, S. L. D. ten Haaf, T. Dvir, and M. Wimmer, Enhancing the excitation gap of a quantum-dot-based kitaev chain, *Commun. Phys.* **7**, 235 (2024).
- [34] R. S. Souto, A. Tsintzis, M. Leijnse, and J. Danon, Probing majorana localization in minimal kitaev chains through a quantum dot, *Phys. Rev. Res.* **5**, 043182 (2023).
- [35] R. Koch, D. van Driel, A. Bordin, J. L. Lado, and E. Greplova, Adversarial hamiltonian learning of quantum dots in a minimal kitaev chain, *Phys. Rev. Appl.* **20**, 044081 (2023).
- [36] B. Pandey, N. Kaushal, G. Alvarez, and E. Dagotto, Majorana zero modes in y-shape interacting kitaev wires, *npj Quantum Materials* **8**, 51 (2023).
- [37] A. M. Bozkurt, S. Miles, S. L. ten Haaf, C.-X. Liu, F. Hassler, and M. Wimmer, Interaction-induced strong zero modes in short quantum dot chains with time-reversal symmetry, [arXiv:2405.14940](https://arxiv.org/abs/2405.14940) (2024).
- [38] S. Miles, D. van Driel, M. Wimmer, and C.-X. Liu, Kitaev chain in an alternating quantum dot-andreev bound state array, *Phys. Rev. B* **110**, 024520 (2024).
- [39] J. D. T. Luna, A. M. Bozkurt, M. Wimmer, and C.-X. Liu, Flux-tunable Kitaev chain in a quantum dot array, *SciPost Phys. Core* **7**, 065 (2024).
- [40] C.-X. Liu, S. Miles, A. Bordin, S. L. ten Haaf, A. M. Bozkurt, and M. Wimmer, Protocol for scaling up a sign-ordered kitaev chain without magnetic flux control, [arXiv:2407.04630](https://arxiv.org/abs/2407.04630) (2024).
- [41] D. van Driel, R. Koch, V. P. Sietses, S. L. ten Haaf, C.-X. Liu, F. Zatelli, B. Roovers, A. Bordin, N. van Loo, G. Wang, *et al.*, Cross-platform autonomous control of minimal kitaev chains, [arXiv:2405.04596](https://arxiv.org/abs/2405.04596) (2024).
- [42] Z.-H. Liu, C. Zeng, and H. Q. Xu, Coupling of quantum-dot states via elastic cotunneling and crossed andreev reflection in a minimal kitaev chain, *Phys. Rev. B* **110**, 115302 (2024).
- [43] M. Ezawa, Even-odd effect on robustness of majorana edge states in short kitaev chains, *Phys. Rev. B* **109**, L161404 (2024).
- [44] W. Samuelson, V. Svensson, and M. Leijnse, Minimal quantum dot based kitaev chain with only local superconducting proximity effect, *Phys. Rev. B* **109**, 035415 (2024).
- [45] J. Benestad, A. Tsintzis, R. S. Souto, M. Leijnse, E. van Nieuwenburg, and J. Danon, Machine-learned tuning of artificial kitaev chains from tunneling spectroscopy measurements, *Phys. Rev. B* **110**, 075402 (2024).
- [46] V. Svensson and M. Leijnse, Quantum dot based kitaev chains: Majorana quality measures and scaling with increasing chain length, *Phys. Rev. B* **110**, 155436 (2024).
- [47] R. S. Souto, V. V. Baran, M. Nitsch, L. Maffi, J. Paaske, M. Leijnse, and M. Burrello, Majorana modes in quantum dots coupled via a floating superconducting island, [arXiv:2411.07068](https://arxiv.org/abs/2411.07068) (2024).
- [48] D. M. Pino, R. S. Souto, and R. Aguado, Minimal kitaev-transmon qubit based on double quantum dots, *Phys. Rev. B* **109**, 075101 (2024).
- [49] R. S. Souto and R. Aguado, Subgap states in semiconductor-superconductor devices for quantum technologies: Andreev qubits and minimal majorana chains, [arXiv:2404.06592](https://arxiv.org/abs/2404.06592) (2024).
- [50] M. Nitsch, L. Maffi, V. V. Baran, R. S. Souto, J. Paaske, M. Leijnse, and M. Burrello, The poor man's majorana tetron, [arXiv:2411.11981](https://arxiv.org/abs/2411.11981) (2024).
- [51] M. Luethi, H. F. Legg, D. Loss, and J. Klinovaja, From perfect to imperfect poor man's majoranas in minimal kitaev chains, *Phys. Rev. B* **110**, 245412 (2024).
- [52] M. Luethi, H. F. Legg, D. Loss, and J. Klinovaja, The fate of poor man's majoranas in the long kitaev chain limit, [arXiv:2408.10030](https://arxiv.org/abs/2408.10030) (2024).
- [53] Á. Gómez-León, M. Schirò, and O. Dmytruk, High-quality poor man's majorana bound states from cavity embedding, [arXiv:2407.12088](https://arxiv.org/abs/2407.12088) (2024).
- [54] B. Pandey, G. Alvarez, E. Dagotto, and R.-X. Zhang, Crystalline-symmetry-protected majorana modes in coupled quantum dots, [arXiv:2407.00158](https://arxiv.org/abs/2407.00158) (2024).
- [55] M. Alvarado, A. L. Yeyati, R. Aguado, and R. S. Souto, Interplay between majorana and shiba states in

- a minimal kitaev chain coupled to a superconductor, [arXiv:2407.07050 \(2024\)](#).
- [56] C.-X. Liu, H. Pan, F. Setiawan, M. Wimmer, and J. D. Sau, Fusion protocol for majorana modes in coupled quantum dots, *Phys. Rev. B* **108**, 085437 (2023).
- [57] P. Boross and A. Pályi, Braiding-based quantum control of a majorana qubit built from quantum dots, *Phys. Rev. B* **109**, 125410 (2024).
- [58] B. Pandey, S. Okamoto, and E. Dagotto, Nontrivial fusion of majorana zero modes in interacting quantum-dot arrays, *Phys. Rev. Res.* **6**, 033314 (2024).
- [59] A. Tsintzis, R. S. Souto, K. Flensberg, J. Danon, and M. Leijnse, Majorana qubits and non-abelian physics in quantum dot-based minimal kitaev chains, *PRX Quantum* **5**, 010323 (2024).
- [60] J. D. Sau, D. J. Clarke, and S. Tewari, Controlling non-abelian statistics of majorana fermions in semiconductor nanowires, *Phys. Rev. B* **84**, 094505 (2011).
- [61] B. van Heck, A. R. Akhmerov, F. Hassler, M. Burrello, and C. W. J. Beenakker, Coulomb-assisted braiding of majorana fermions in a josephson junction array, *New Journal of Physics* **14**, 035019 (2012).
- [62] T. Karzig, F. Pientka, G. Refael, and F. von Oppen, Shortcuts to non-abelian braiding, *Phys. Rev. B* **91**, 201102 (2015).
- [63] M. Hell, J. Danon, K. Flensberg, and M. Leijnse, Time scales for Majorana manipulation using Coulomb blockade in gate-controlled superconducting nanowires, *Phys. Rev. B* **94**, 035424 (2016).
- [64] P. Bonderson, M. Freedman, and C. Nayak, Measurement-only topological quantum computation, *Phys. Rev. Lett.* **101**, 010501 (2008).
- [65] S. Plugge, A. Rasmussen, R. Egger, and K. Flensberg, Majorana box qubits, *New Journal of Physics* **19**, 012001 (2017).
- [66] T. Karzig, C. Knapp, R. M. Lutchyn, P. Bonderson, M. B. Hastings, C. Nayak, J. Alicea, K. Flensberg, S. Plugge, Y. Oreg, C. M. Marcus, and M. H. Freedman, Scalable designs for quasiparticle-poisoning-protected topological quantum computation with Majorana zero modes, *Phys. Rev. B* **95**, 235305 (2017).
- [67] J. Alicea, Y. Oreg, G. Refael, F. von Oppen, and M. P. A. Fisher, Non-abelian statistics and topological quantum information processing in 1d wire networks, *Nature Physics* **7**, 412 EP (2011).
- [68] J. Liu, W. Chen, M. Gong, Y. Wu, and X. Xie, Minimal setup for non-abelian braiding of majorana zero modes, *Science China Physics, Mechanics & Astronomy* **64**, 117811 (2021).
- [69] L. Xu, J. Bai, W. Feng, and X.-Q. Li, Dynamics simulation of braiding two majorana zero modes via a quantum dot, *Physical Review B* **108**, 115411 (2023).
- [70] D. J. Clarke, J. D. Sau, and S. Das Sarma, Probability and braiding statistics in Majorana nanowires, *Phys. Rev. B* **95**, 155451 (2017).
- [71] T. Hensgens, T. Fujita, L. Janssen, X. Li, C. J. Van Diepen, C. Reichl, W. Wegscheider, S. Das Sarma, and L. M. K. Vandersypen, Quantum simulation of a fermi-hubbard model using a semiconductor quantum dot array, *Nature* **548**, 70 (2017).
- [72] T.-K. Hsiao, P. Cova Fariña, S. D. Oosterhout, D. Jirovec, X. Zhang, C. J. van Diepen, W. I. L. Lawrie, C.-A. Wang, A. Sammak, G. Scappucci, M. Veldhorst, E. Demler, and L. M. K. Vandersypen, Exciton transport in a germanium quantum dot ladder, *Phys. Rev. X* **14**, 011048 (2024).
- [73] F. van Riggelen, N. W. Hendrickx, W. I. L. Lawrie, M. Russ, A. Sammak, G. Scappucci, and M. Veldhorst, A two-dimensional array of single-hole quantum dots, *Applied Physics Letters* **118**, 044002 (2021).
- [74] F. Arute, K. Arya, R. Babbush, D. Bacon, J. C. Bardin, R. Barends, R. Biswas, S. Boixo, F. G. S. L. Brandao, D. A. Buell, B. Burkett, Y. Chen, Z. Chen, B. Chiaro, R. Collins, W. Courtney, A. Dunsworth, E. Farhi, B. Foxen, A. Fowler, C. Gidney, M. Giustina, R. Graff, K. Guerin, S. Habegger, M. P. Harrigan, M. J. Hartmann, A. Ho, M. Hoffmann, T. Huang, T. S. Humble, S. V. Isakov, E. Jeffrey, Z. Jiang, D. Kafri, K. Kechedzhi, J. Kelly, P. V. Klimov, S. Knysh, A. Korotkov, F. Kostritsa, D. Landhuis, M. Lindmark, E. Lucero, D. Lyakh, S. Mandrà, J. R. McClean, M. McEwen, A. Megrant, X. Mi, K. Michielsen, M. Mohseni, J. Mutus, O. Naaman, M. Neeley, C. Neill, M. Y. Niu, E. Ostby, A. Petukhov, J. C. Platt, C. Quintana, E. G. Rieffel, P. Roushan, N. C. Rubin, D. Sank, K. J. Satzinger, V. Smelyanskiy, K. J. Sung, M. D. Trevithick, A. Vainsencher, B. Villalonga, T. White, Z. J. Yao, P. Yeh, A. Zalcman, H. Neven, and J. M. Martinis, Quantum supremacy using a programmable superconducting processor, *Nature* **574**, 505 (2019).
- [75] H. Pan, S. D. Sarma, and C.-X. Liu, Rabi and ramsay oscillations of a majorana qubit in a quantum dot-superconductor array, [arXiv:2407.16750 \(2024\)](#).
- [76] C. Knapp, M. Zaletel, D. E. Liu, M. Cheng, P. Bonderson, and C. Nayak, The nature and correction of diabatic errors in anyon braiding, *Phys. Rev. X* **6**, 041003 (2016).
- [77] X. Hu and S. Das Sarma, Charge-fluctuation-induced dephasing of exchange-coupled spin qubits, *Phys. Rev. Lett.* **96**, 100501 (2006).
- [78] K. D. Petersson, J. R. Petta, H. Lu, and A. C. Gosard, Quantum coherence in a one-electron semiconductor charge qubit, *Phys. Rev. Lett.* **105**, 246804 (2010).
- [79] O. E. Dial, M. D. Shulman, S. P. Harvey, H. Bluhm, V. Umansky, and A. Yacoby, Charge noise spectroscopy using coherent exchange oscillations in a singlet-triplet qubit, *Phys. Rev. Lett.* **110**, 146804 (2013).
- [80] P. Scarlino, J. H. Ungerer, D. J. van Woerkom, M. Mancini, P. Stano, C. Müller, A. J. Landig, J. V. Koski, C. Reichl, W. Wegscheider, T. Ihn, K. Ensslin, and A. Wallraff, In situ tuning of the electric-dipole strength of a double-dot charge qubit: Charge-noise protection and ultrastrong coupling, *Phys. Rev. X* **12**, 031004 (2022).
- [81] E. J. Connors, J. Nelson, L. F. Edge, and J. M. Nichol, Charge-noise spectroscopy of si/sige quantum dots via dynamically-decoupled exchange oscillations, *Nature Communications* **13**, 940 (2022).
- [82] R. E. Throckmorton and S. Das Sarma, Crosstalk and charge-noise-induced multiqubit decoherence in exchange-coupled quantum dot spin qubit arrays, *Phys. Rev. B* **105**, 245413 (2022).
- [83] G. Burkard, T. D. Ladd, A. Pan, J. M. Nichol, and J. R. Petta, Semiconductor spin qubits, *Rev. Mod. Phys.* **95**, 025003 (2023).
- [84] E. Paladino, Y. M. Galperin, G. Falci, and B. L. Altshuler, $1/f$ noise: Implications for solid-state quantum information, *Rev. Mod. Phys.* **86**, 361 (2014).
- [85] G. Ithier, E. Collin, P. Joyez, P. J. Meeson, D. Vion,

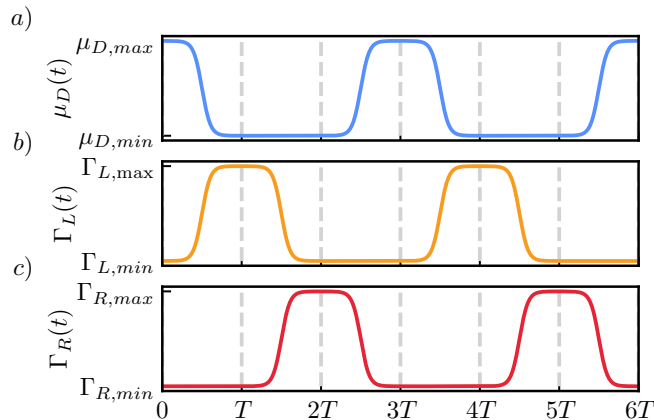


FIG. 8. Parameters of the double braid protocol depending on time. (a) chemical potential $\mu_D(t)$ of the ancillary dot. (c) and (d), tunnel coupling of the ancillary dot to the left and right Kitaev chain respectively.

- D. Esteve, F. Chiarello, A. Shnirman, Y. Makhlin, J. Schrieffer, and G. Schön, Decoherence in a superconducting quantum bit circuit, *Phys. Rev. B* **72**, 134519 (2005).
- [86] P. Boross and A. Pályi, Dephasing of majorana qubits due to quasistatic disorder, *Phys. Rev. B* **105**, 035413 (2022).
- [87] M. Aghaee, A. A. Ramirez, Z. Alam, R. Ali, M. Andrzejczuk, A. Antipov, M. Astafev, A. Barzegar, B. Bauer, J. Becker, *et al.*, Interferometric single-shot parity measurement in an inas-al hybrid device, [arXiv:2401.09549](https://arxiv.org/abs/2401.09549) (2024).
- [88] S. Miles, F. Zatelli, A. M. Bozkurt, M. Wimmer, and C.-X. Liu, [Braiding Majoranas in a linear quantum dot-superconductor array: Mitigating the errors from Coulomb repulsion and residual tunneling](https://arxiv.org/abs/2501.03728) (2025).
- [89] J. R. Johansson, P. D. Nation, and F. Nori, Qutip: An open-source python framework for the dynamics of open quantum systems, *Computer physics communications* **183**, 1760 (2012).
- [90] I. A. Day, S. Miles, H. K. Kerstens, D. Varjas, and A. R. Akhmerov, Pymablock: an algorithm and a package for quasi-degenerate perturbation theory, [arXiv:2404.03728](https://arxiv.org/abs/2404.03728) (2024).

Appendix A: Details of the numerical calculation

In this appendix we expand on the numerical tools used to generate the figures of this work. The associated repository containing all codes used for this work can be found in Ref. [88].

To simulate braiding in the setup described in Sec. II, we use the QUTIP [89] Python package to calculate the time evolution. The perturbation theory results of Sec. IV and App. B are generated with Pymablock [90].

To model the time dependent coupling between the different Majoranas (cf. Fig. 1 c)) we have to specify the profiles for μ_D , Γ_L , and Γ_R . We model each parameter by the time dependent function

$$p(\tilde{t}, p_{min}, p_{max}, \sigma_p) = (p_{max} - p_{min}) \left(\frac{1}{2} + \tanh\left(\frac{\tilde{t} - \frac{T}{2}}{t_{ramp}}\right) - \tanh\left(\frac{\tilde{t} - \frac{3T}{2}}{t_{ramp}}\right) + \tanh\left(\frac{\tilde{t} - \frac{7T}{2}}{t_{ramp}}\right) \right), \quad (\text{A1})$$

$$\tilde{t} = (t + t_0) \pmod{3T}. \quad (\text{A2})$$

Choosing $t_0 = T$ generates the profile of μ_D , $t_0 = 0$ Γ_L , and $t_0 = 2T$ yields Γ_R . The resulting profiles can be found in Fig. 8.

The parameters for the time evolution need to obey the adiabaticity constraint $T \sim h/\Gamma_0$ of the protocol. To find parameters for the time evolution that both, obey the adiabaticity constraint and deliver unit fidelities, we construct the full Hamiltonian as given in Eq. (1). We fix all the parameters at their optimal point ($t_L = \Delta_L = t_R = \Delta_R = 5\Gamma_0$, and $\varphi = \pi$). We choose the stepsize of the time discretization to $\Delta t = 0.2h/\Gamma$ corresponding to $\sim 0.1ns$ given typical coupling strengths of $\Gamma_0 \sim 10\mu eV$. We then optimize numerically for T and the ramping time t_{ramp} by demanding that $P_{|oo\rangle}(3T) = 1/2$ and $P_{|oo\rangle}(6T) = 1$. This results in $(T_{opt}, t_{ramp, opt}) = (200.54, 21.21)h/\Gamma_0$ which is our default parameter choice unless specified otherwise. When changing T away from the optimized value, we have to adjust the ramping time accordingly. This we do by letting $t_{ramp} \rightarrow T t_{ramp, opt}/T_{opt}$ such as to coincide with the optimal choice when $T = T_{opt}$.

Appendix B: Effective odd parity Hamiltonian and excitation minimum

1. Effective Hamiltonian in odd and even parity sectors

As discussed in the main text, it suffices to only consider a single PMM coupled to the ancillary dot to understand the physics relevant for the Coulomb repulsion. The Hamiltonian of this system reads

$$\begin{aligned}
H_{LD} &= H_{K,L} + H_{\text{tunn},L} + H_{C,L} + H_D, \\
H_{K,L} &= \mu_{L1}n_{L1} + \mu_{L2}n_{L2} + tc_{L2}^\dagger c_{L1} + \Delta c_{L2}c_{L1} + h.c., \\
H_D &= \mu_D n_D, \\
H_{\text{tunn},L} &= \Gamma_L \left(c_D^\dagger c_{L2} + c_{L2}^\dagger c_D \right), \\
H_{C,L} &= U_L n_D n_{L2}.
\end{aligned} \tag{B1}$$

Since the system preserves the total fermionic parity we can separate the Hilbert space into the even and odd total parity subspaces. In the even parity sector consisting of the basis $|e_L, 0_D\rangle, |o_L, 1_D\rangle, |e'_L, 0_D\rangle, |o'_L, 1_D\rangle$ we find Eq. (16), i.e.

$$H_{LD}^{(even)} = \begin{pmatrix} 0 & \frac{\Gamma_L}{2} & 0 & \frac{\Gamma_L}{2} \\ \frac{\Gamma_L}{2} & \mu_D + \frac{U_L}{2} & \frac{\Gamma_L}{2} & -\frac{U_L}{2} \\ 0 & \frac{\Gamma_L}{2} & 2\Delta_L & \frac{\Gamma_L}{2} \\ \frac{\Gamma_L}{2} & -\frac{U_L}{2} & \frac{\Gamma_L}{2} & 2\Delta_L + \mu_D + \frac{U_L}{2} \end{pmatrix}. \tag{B2}$$

In the odd parity basis, consisting of $|e_L, 1_D\rangle, |o_L, 0_D\rangle, |e'_L, 1_D\rangle, |o'_L, 0_D\rangle$, we find through an analogous calculation the Hamiltonian

$$H_{LD}^{(odd)} = \begin{pmatrix} \frac{U_L}{2} + \mu_D & \frac{\Gamma_L}{2} & \frac{U_L}{2} & -\frac{\Gamma_L}{2} \\ \frac{\Gamma_L}{2} & 0 & -\frac{\Gamma_L}{2} & 0 \\ \frac{U_L}{2} & -\frac{\Gamma_L}{2} & \frac{U_L}{2} + 2\Delta_L + \mu_D & \frac{\Gamma_L}{2} \\ -\frac{\Gamma_L}{2} & 0 & \frac{\Gamma_L}{2} & 2\Delta_L \end{pmatrix}, \tag{B3}$$

Due to the aforementioned parity conservation the spectrum will be strongly degenerate between parity sectors.

2. Excitation gap minimum

The excitation gap can be found through Eq. (17) from the main text. We find the eigenvalues of the effective Hamiltonian to be

$$\epsilon_{\pm} = \frac{1}{2} \left(\mu_D + \frac{U_L}{2} + \Delta_L - \lambda \right) \pm \sqrt{\frac{\Gamma_L^2}{4} (a+b)^2 + \frac{1}{4} \left(\mu_D + \frac{U_L}{2} + \Delta_L - \lambda \right)^2}. \tag{B4}$$

The excitation gap is the difference of these two eigenvalues given as

$$\Delta\epsilon = \sqrt{\Gamma_L^2 (a+b)^2 + \left(\mu_D + \frac{U_L}{2} + \Delta_L - \lambda \right)^2} \tag{B5}$$

Inspecting Eq. (B5), it becomes apparent that the excitation gap becomes minimal exactly for the predicted value of $\mu_D = \mu_D^*$ as given in Eq. (18). We find the value of the excitation gap to be

$$\Delta\epsilon_{\min} = \Gamma_L \frac{\sqrt{\sqrt{4\Delta_L^2 + U_L^2} + 2\Delta_L} + \sqrt{\sqrt{4\Delta_L^2 + U_L^2} - 2\Delta_L}}{\sqrt{2}(4\Delta_L^2 + U_L^2)^{1/4}} \tag{B6}$$

for a single Kitaev chain attached to the ancillary dot.

Appendix C: Calculation of the non-Abelian Berry phase

In this section, we show the details for calculating the non-Abelian Berry's phase in the presence of residual couplings. The calculation is similar in spirit to Ref. [61], but we generalize it to asymmetric couplings. The Hamiltonian is given by

$$H = \sum_{k=1}^3 \Delta_k i\gamma_0 \gamma_k, \quad (\text{C1})$$

which involves four Majoranas in total. We thus define fermionic operators as below

$$f_1 = (\gamma_1 + i\gamma_2)/2, \quad f_2 = (\gamma_0 + i\gamma_3)/2, \quad (\text{C2})$$

so that we can further define the four-dimensional Fock space as

$$\begin{aligned} |00\rangle, \\ |10\rangle &= f_1^\dagger |00\rangle, \\ |01\rangle &= f_2^\dagger |00\rangle, \\ |11\rangle &= f_1^\dagger f_2^\dagger |00\rangle. \end{aligned} \quad (\text{C3})$$

As such, the Hamiltonian can now be written as

$$H = \begin{pmatrix} |00\rangle \\ |11\rangle \\ |10\rangle \\ |01\rangle \end{pmatrix}^T \begin{pmatrix} -\Delta_3 & i\Delta_1 + \Delta_2 & 0 & 0 \\ -i\Delta_1 + \Delta_2 & \Delta_3 & 0 & 0 \\ 0 & 0 & -\Delta_3 & -i\Delta_1 + \Delta_2 \\ 0 & 0 & i\Delta_1 + \Delta_2 & \Delta_3 \end{pmatrix} \begin{pmatrix} \langle 00| \\ \langle 11| \\ \langle 10| \\ \langle 01| \end{pmatrix}. \quad (\text{C4})$$

We note that here the even- and odd-parity subspaces are block diagonalized due to fermion parity conservation. The dimension of each subspace is two.

We first focus on the even-parity subspace, where the ground-state energy is

$$E_{e,gs} = -\varepsilon = -\sqrt{\Delta_1^2 + \Delta_2^2 + \Delta_3^2}, \quad (\text{C5})$$

and the wavefunction is

$$|e\rangle = \sqrt{\frac{\varepsilon - \Delta_3}{2\varepsilon}} \begin{pmatrix} -i\frac{\Delta_3 + \varepsilon}{\Delta_1 + i\Delta_2} \\ 1 \end{pmatrix}. \quad (\text{C6})$$

Using sympy, we obtain that

$$\begin{aligned} A_{e,1} &= \langle e | \frac{d}{d\Delta_1} | e \rangle = \frac{\Delta_2}{\Delta_1^2 + \Delta_2^2} \frac{i(\varepsilon + \Delta_3)}{2\varepsilon}, \\ A_{e,2} &= \langle e | \frac{d}{d\Delta_2} | e \rangle = \frac{-\Delta_1}{\Delta_1^2 + \Delta_2^2} \frac{i(\varepsilon + \Delta_3)}{2\varepsilon}, \\ A_{e,3} &= 0. \end{aligned} \quad (\text{C7})$$

Using the same calculation method, we find that

$$E_{o,gs} = -\varepsilon = -\sqrt{\Delta_1^2 + \Delta_2^2 + \Delta_3^2}, \quad (\text{C8})$$

and the wavefunction is

$$|o\rangle = \sqrt{\frac{\varepsilon - \Delta_3}{2\varepsilon}} \begin{pmatrix} i\frac{\Delta_3 + \varepsilon}{\Delta_1 - i\Delta_2} \\ 1 \end{pmatrix}. \quad (\text{C9})$$

Note that the odd-parity wavefunction is different from the even one by $i \rightarrow -i$. Thus the signs of the Berry connections are simply reversed, i.e.

$$\vec{A}_o = -\vec{A}_e. \quad (\text{C10})$$

Due to parity conservation, the matrix elements between even- and odd-parity states are zero.

The unitary evolution for the Majorana braiding is defined as

$$U = \exp \left(- \oint_c \sum_k A_k d\Delta_k \right). \quad (\text{C11})$$

Here the Berry connection shown in Eq. (C7) is singular when $\Delta_1 = \Delta_2 = 0$ because of the presence of a term $\Delta_1/(\Delta_1^2 + \Delta_2^2)$. To avoid the singular points, we assume that the couplings have some residual amplitudes even when they are “switched off”, i.e., $\eta_k \leq \Delta_k \leq \Gamma$. Here we first assume that the maximal strengths of all Δ_k 's are assumed to be the same and equal to Γ to simplify the calculation. In particular, in the three-step braid operation, we assume six contours in the parameter path as below

$$\begin{aligned} C1 &: (\eta_1, \eta_2, \Gamma) \rightarrow (\Gamma, \eta_2, \Gamma), \\ C2 &: (\Gamma, \eta_2, \Gamma) \rightarrow (\Gamma, \eta_2, \eta_3), \\ C3 &: (\Gamma, \eta_2, \eta_3) \rightarrow (\Gamma, \Gamma, \eta_3), \\ C4 &: (\Gamma, \Gamma, \eta_3) \rightarrow (\eta_1, \Gamma, \eta_3), \\ C5 &: (\eta_1, \Gamma, \eta_3) \rightarrow (\eta_1, \Gamma, \Gamma), \\ C6 &: (\eta_1, \Gamma, \Gamma) \rightarrow (\eta_1, \eta_2, \Gamma), \end{aligned} \quad (\text{C12})$$

where each bracket denotes $(\Delta_1, \Delta_2, \Delta_3)$. We note that only 4 out of the 6 contours contribute to the Berry's phase. We name them as $C1 \rightarrow I_1, C4 \rightarrow I_2, C3 \rightarrow I_3, C6 \rightarrow I_4$.

$$- \oint_c \sum_k A_k d\Delta_k = \left(\frac{-i}{2} \right) I = \left(\frac{-i}{2} \right) (I_1 + I_2 + I_3 + I_4), \quad (\text{C13})$$

In particular

$$I_1 = \int_{\eta_1}^{\Gamma} A_1(\Delta_1, \eta_2, \Gamma) d\Delta_1 = \int_{\eta_1}^{\Gamma} d\Delta_1 \frac{\eta_2}{\Delta_1^2 + \eta_2^2} \left(1 + \frac{\Gamma}{\sqrt{\Delta_1^2 + \Gamma^2}} \right). \quad (\text{C14})$$

Here the first integral is

$$I_{11} = \int_{\eta_1}^{\Gamma} d\Delta_1 \frac{\eta_2}{\Delta_1^2 + \eta_2^2} = \int_a^b dx \frac{1}{x^2 + 1} = \text{atan}(b) - \text{atan}(a), \quad (\text{C15})$$

where $b = \Gamma/\eta_2$ and $a = \eta_1/\eta_2$. The second part is

$$I_{12} = \int_{\eta_1}^{\Gamma} d\Delta_1 \frac{\eta_2}{\Delta_1^2 + \eta_2^2} \frac{\Gamma}{\sqrt{\Delta_1^2 + \Gamma^2}} = \int_a^b dx \frac{1}{x^2 + 1} \frac{b}{\sqrt{x^2 + b^2}}. \quad (\text{C16})$$

We obtain the result for the indefinite integral as given below

$$\int dx \frac{1}{x^2 + 1} \frac{b}{\sqrt{x^2 + b^2}} = \frac{b}{\sqrt{1 - b^2}} \tanh^{-1} \left(\frac{\sqrt{1 - b^2}}{\sqrt{b^2 + x^2}} x \right) \approx \text{atan} \left(\frac{bx}{\sqrt{b^2 + x^2}} \right), \quad (\text{C17})$$

where we assume $b \gg 1$ and use the relation of $\tanh^{-1}(ib) = i \text{atan}(b)$. Therefore we have

$$I_{12} = \text{atan} \left(\frac{b}{\sqrt{2}} \right) - \text{atan}(a) \approx \frac{\pi}{2} - \frac{\sqrt{2}}{b} - \text{atan}(a), \quad (\text{C18})$$

where we consider $a \sim O(1) \ll b$ and use the identity of $\text{atan}(x) = \pi/2 - \text{atan}(1/x)$. We thus have

$$I_1 = \text{atan}(\Gamma/\eta_2) - 2 \text{atan}(\eta_1/\eta_2) + \frac{\pi}{2} - \frac{\sqrt{2}\eta_2}{\Gamma}. \quad (\text{C19})$$

Next, the second integral is

$$\begin{aligned} I_2 &= \int_{\Gamma}^{\eta_1} A_1(\Delta_1, \Gamma, \eta_3) d\Delta_1 = - \int_{\eta_1}^{\Gamma} d\Delta_1 \frac{\Gamma}{\Delta_1^2 + \Gamma^2} \left(1 + \frac{\eta_3}{\sqrt{\Delta_1^2 + \Gamma^2}} \right) \\ &= - \left[\text{atan}(1) - \text{atan}(\eta_1/\Gamma) + \frac{\eta_3}{\sqrt{2}\Gamma} \right]. \end{aligned} \quad (\text{C20})$$

And the third integral is

$$\begin{aligned} I_3 &= \int_{\eta_2}^{\Gamma} A_2(\Gamma, \Delta_2, \eta_3) d\Delta_2 = \int_{\eta_2}^{\Gamma} d\Delta_2 \frac{-\Gamma}{\Delta_2^2 + \Gamma^2} \left(1 + \frac{\eta_3}{\sqrt{\Delta_2^2 + \Gamma^2}} \right) \\ &= - \left[\text{atan}(1) - \text{atan}(\eta_2/\Gamma) + \frac{\eta_3}{\sqrt{2}\Gamma} \right]. \end{aligned} \quad (\text{C21})$$

Lastly, the fourth integral is

$$\begin{aligned} I_4 &= \int_{\Gamma}^{\eta_2} A_2(\eta_1, \Delta_2, \Gamma) d\Delta_2 \\ &= \text{atan}(\Gamma/\eta_1) + \frac{\pi}{2} - \frac{\sqrt{2}\eta_1}{\Gamma} - 2 \text{atan}(\eta_2/\eta_1). \end{aligned} \quad (\text{C22})$$

After summing them up, we obtain

$$I = \sum_{i=1}^4 I_i = \frac{\pi}{2} - \frac{\sqrt{2}}{\Gamma} (\eta_1 + \eta_2 + \eta_3), \quad (\text{C23})$$

giving the unitary evolution matrix as below

$$U = \exp\left(\frac{-i}{2} I \sigma_z\right) = \exp\left(-i \left(\frac{\pi}{4} - \epsilon\right) \sigma_z\right), \quad (\text{C24})$$

where

$$\epsilon = \frac{(\eta_1 + \eta_2 + \eta_3)}{\sqrt{2}\Gamma} + O(\eta_i/\Gamma)^2. \quad (\text{C25})$$

In the notation for braiding Majoranas in Kitaev chains, it becomes

$$U_{\text{braid}} = \exp\left(-i \left(\frac{\pi}{2} - \epsilon\right) \gamma_2 \gamma_3\right), \quad (\text{C26})$$

where

$$\epsilon = \frac{(\Gamma_{L,\min} + \Gamma_{R,\min} + \mu_{D,\min})}{\sqrt{2}\Gamma} + O(\eta_i/\Gamma)^2 \quad (\text{C27})$$

A similar calculation can be performed assuming $\Delta_{1,\max} = \Delta_{2,\max} \ll \Delta_{3,\max}$. It yields

$$\epsilon = \frac{1}{\sqrt{2}} \left(\frac{\Gamma_{L,\min}}{\Gamma} + \frac{\Gamma_{R,\min}}{\Gamma} + \frac{\sqrt{2}\mu_{D,\min}}{\Gamma} \right) + O(\eta_i/\Gamma, \Gamma/\mu_{D,\max}). \quad (\text{C28})$$